Journal of Alloys and Compounds 509 (2011) 3606–3612

Contents lists available at ScienceDirect

Journal of Alloys and Compounds

journal homepage: www.elsevier.com/locate/jallcom

Tunable deep-level emission in ZnO nanoparticles via yttrium doping

Jinghai Yang[a,b,c,*], Rui Wang[a,b], Lili Yang[a,b], Jihui Lang[a,b], Maobin Wei[a,b], Ming Gao[a,b], Xiaoyan Liu[a,b], Jian Cao[a,b], Xue Li[a,b], Nannan Yang[a,b]

[a] Institute of Condensed State Physics, Jilin Normal University, Siping 136000, PR China
[b] Key Laboratory of Functional Materials Physics and Chemistry (Jilin Normal University), Ministry of Education, Siping 136000, PR China
[c] National Laboratory of Superhard Materials, Jilin University, Changchun 130012, China

ARTICLE INFO

Article history:
Received 25 July 2010
Received in revised form
11 December 2010
Accepted 15 December 2010
Available online 23 December 2010

Keywords:
ZnO nanoparticles
Yttrium-doped
Sol–gel technique
Optical properties

ABSTRACT

Yttrium-doped ZnO nanoparticles ($Zn_{1-x}Y_xO$, $x = 0$, 0.03, 0.05) were synthesized by sol–gel technique. The effects of yttrium doping concentration on the structures, morphologies and optical properties of as-synthesized $Zn_{1-x}Y_xO$ nanoparticles were investigated in detail. The results from structural characterizations clearly demonstrated that yttrium ions were successfully doped into the crystal lattice of ZnO matrix. Besides a UV emission centered at ~383 nm, the PL spectra of all the samples exhibited a broad deep-level emission, which can be deconvoluted into two Gauss peaks centered at 539 nm (P1) and 598 nm (P2), respectively. As the concentration of Y doping increased from 0% to 5%, the peak position with maximum intensity in deep-level emission band was gradually tuned from 539 nm to 598 nm and the relative intensity ratio of I_{P1}/I_{P2} also decreased step by step, which revealed a unique optical property of yttrium-doped ZnO nanoparticles.

1. Introduction

ZnO is one of II–VI compound semiconductors with a wide direct band gap of 3.37 eV and a large exciton binding energy of 60 meV at room temperature, which makes it a promising candidate for highly efficient ultraviolet light-emitting diodes (LED) and ultraviolet lasers [1–3]. But it is worth to note that ZnO is also a kind of potential materials for fabricating white LEDs due to its broad deep-level emission in the visible wavelength range. This means that white LEDs, which is a combination of UV-LED and white phosphor, can be fabricated by only using ZnO based materials without organic phosphors. It is well-known that the possibility of practical application of any semiconductor lies on the effective manipulation of its physical properties. No doubt, doping selective elements into ZnO matrix offers an effective method to realize it. Recently, rare-earth (RE) ion doped ZnO nanostructures have attracted intensive interests, since RE elements have great possibility to efficiently modulate the emission in the visible range due to their unique optical properties and excellent qualification to be radiative centers [4–8].

Until now, ZnO nanostructures have been fabricated by chemical solution deposition method [9,10], physical vapor deposition [11–14], pulsed laser deposition [15] and sol–gel process [16–19]. Among these methods, the sol–gel technique has great advantages due to its simplicity, safety, high turnout and low cost. Recently, ZnO thin films with doping Er or Y have been successfully prepared by the sol–gel process [20–24]. However, the synthesis of Y-doped ZnO nanoparticles by the sol–gel method has been rarely reported [25,26]. Spontaneously, the effects of Y-doping on the structural and optical properties of ZnO are not clear yet due to the limited investigation. Hence, more attention should be paid onto the Y-doped ZnO nanostructures systems.

In this paper, we successfully prepared the Y-doped ZnO nanoparticles with the sol–gel method. We also investigated in detail the effects of Y doping on the structures, morphologies, Raman and specially photoluminescence (PL) properties of ZnO nanoparticles.

2. Experimental

All the starting materials were analytical grade and were used without further purification. Zinc nitrate hexahydrate ($Zn(NO_3)_2{\cdot}6H_2O$) and yttrium nitrate hexahydrate ($Y(NO_3)_3{\cdot}6H_2O$) were used as Zn and Y sources, respectively. Citric acid ($C_6H_8O_7{\cdot}H_2O$) was used as a complexing agent for forming reticulated complexes with metal ions. The molar ratio of citric acid to zinc nitrate hexahydrate was maintained at 2.0 and the concentration of zinc nitrate hexahydrate was 0.01 M. $Zn(NO_3)_2{\cdot}6H_2O$, $Y(NO_3)_3{\cdot}6H_2O$ (Y/Zn = 0%, 3%, 5%) and citric acid were dissolved in deionized water, respectively. Yttrium nitrate aqueous solution (10 ml) and citric acid aqueous solution (20 ml) were successively added into zinc nitrate aqueous solution (20 ml) under stirring. The final mixed solution was stirred for 2 h and then put into the drying cabinet for hours at 80 °C to obtain sol. Subsequently, the sol was polymerized to form a gel at 130 °C as amorphous composite precursor. After

* Corresponding author at: Institute of Condensed State Physics, Jilin Normal University, No. 1301, Haifeng Street, Siping 136000, PR China. Tel.: +86 434 3294566; fax: +86 434 3294566.
E-mail address: jhyang1@jlnu.edu.cn (J. Yang).

0925-8388/$ – see front matter © 2010 Elsevier B.V. All rights reserved.
doi:10.1016/j.jallcom.2010.12.102

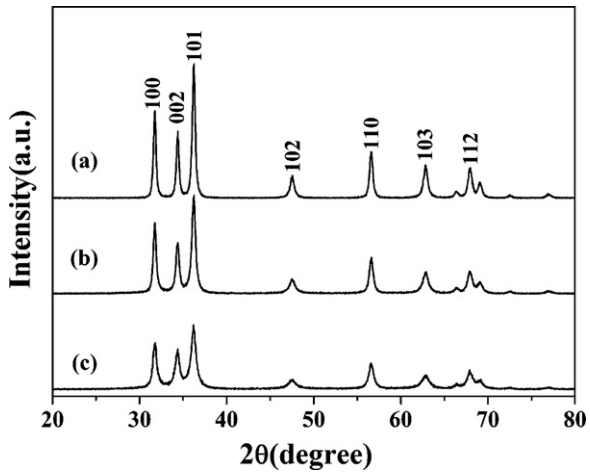

Fig. 1. XRD patterns of the pure and Y-doped ZnO nanoparticles. (a) undoped, (b) $Zn_{0.97}Y_{0.03}O$, and (c) $Zn_{0.95}Y_{0.05}O$.

grinding, the precursor was placed in a ceramic crucible and put into a box furnace at 500 °C for 1 h. Finally, the white powders were obtained after the furnace cooling down to room temperature.

X-ray diffraction (XRD) (MAC Science, MXP18, Japan), transmission electron microscope (TEM) and high-resolution TEM experiment (HETEM) (200 keV, JEM-2100HR, Japan), X-ray photoelectron spectroscopy (XPS) (VG ESCALAB Mark II), photoluminescence (PL) (He–Cd Laser, 325 nm) and Raman spectrometer (Invia-UV, UK) were used to characterize the crystal structures, morphologies, chemical composition and optical properties of ZnO nanoparticles.

3. Results and discussion

Fig. 1(a–c) shows XRD patterns of the pure and Y-doped ZnO nanoparticles ($Zn_{1-x}Y_xO$, $x = 0, 0.03, 0.05$). The diffraction peaks are in good agreement with the standard JCPDS file for ZnO (JCPDS 36-1451, $a = b = 3.249$ Å, $c = 5.206$ Å) and can be indexed as a hexagonal wurtzite structure with $P6_{3mc}$ space group. No other impurities or yttrium oxide phases are observed in all XRD patterns, which means that the yttrium ions would uniformly substitute into the Zn^{2+} or interstitial sites in the ZnO crystal lattices. Moreover, it can be observed that the diffraction peaks of Y-doped ZnO become weaker and broader with increasing the Y doping concentrations, which indicates a decrease in crystallinity and a smaller size of Y-doped ZnO nanoparticles. We can also observe that the (1 0 1) peaks slightly shift to the lower angle side with increasing the Y-doping concentration, since the ionic radius of Y^{3+} (0.89 Å) is larger than that of Zn^{2+} (0.74 Å) [27]. We consider that the decrease of the crystallinity could be mainly attributed to a restrained nucleation rate and subsequently lower growth rate caused by the size difference of Zn and Y ions. We also estimate the average crystal size with Debye–Scherer formula: $D = 0.9\lambda/\beta\cos\theta$, where D is the crystal size, λ is the wavelength of X-ray, θ is the Bragg angle and β is the full width at half maximum (FWHM) on 2θ scale. The average crystal size is approximately 38.5, 30.2 and 19.7 nm corresponding to 0%, 3% and 5% doping concentration, respectively. The incorporated Y atoms probably build obstructions for the movement of grain boundary and limit the grain growth. First of all, the formation of Y–O–Zn precursors is obtained in the sol–gel solution. After sintering at 500 °C, Y ions sitting in the interfaces or grain boundaries between nanoparticles might substitute into the Zn^{2+} sites to lower the interfacial energy of the nanoparticles, which are combined one single wurtzite nanocrystal with two or more ZnO nanoparticles in the crystallization process. Thus, a smaller size of Y-doped ZnO nanoparticles is obtained [28–30].

Fig. 2(a–f) shows the TEM and HETEM images of the $Zn_{1-x}Y_xO$($x = 0, 0.03, 0.05$). From Fig. 2(a–c), we can observe that the sizes of the samples are ~40, ~30 and ~20 nm, which is consistent with the calculated values from XRD patterns. In Fig. 2(a), the pure ZnO nanoparticles exhibit hexagon shapes. The HRTEM images (Fig. 2(d–f)) exhibit a clear lattice spacing of 2.606, 2.608, 2.604 Å, respectively, which matches well with the distance of the (0 0 2) plane of the standard wurtzite-type ZnO structure. With increasing the Y-doping concentrations, the shapes of the samples turn into quasi-spherical one with smooth brim. Normally, ZnO is apt to grow along [0 0 0 1] direction due to its faster growth rate, which also happens in our case in HRTEM images [31–33]. For pure ZnO, this growth tendency is quite obvious which results in a hexagonal structure. For Y-doped ZnO samples, clearly, Y doping does not break this growth tendency and even has no big influence on the wurtzite structures of ZnO because the lattice spacing values of three samples are almost same. However, the Y element will appear in all different growth planes, which probably makes the growth velocity in each direction quite similar so that the Y-doped ZnO exhibit quasi-spherical shapes.

In order to confirm the presence of Y^{3+}, energy dispersion spectrum (EDS) analysis of $Zn_{0.95}Y_{0.05}O$ is shown in Fig. 3. We can see that the nanoparticles are mostly composed of Zn, Y, Cu, and O elements. The existence of Cu signal is due to the Cu TEM grid. The Y:Zn ratio determined from EDS analysis is ~4.76%, which is quite close to the desired Y-doping concentration.

To further determine the chemical composition, XPS technique is used to investigate the $Zn_{0.95}Y_{0.05}O$ nanoparticles. Fig. 4(a) shows the XPS survey spectrum from $Zn_{0.95}Y_{0.05}O$, in which all of the peaks can be ascribed to Zn, Y, O, and C elements as labeled in Fig. 4(a) [34]. It is indicated that there are no other impurities in $Zn_{0.95}Y_{0.05}O$ nanoparticles. We would like to mention that, in the XPS spectrum in Fig. 4, the binding energies have been calibrated by taking the carbon C1s peak (285.0 eV) as reference. The high resolution scans of Zn2p, O1s and Y3d are shown in Fig. 4(b–d). In Fig. 4(b), the peaks located at 1022.1 eV and 1045.4 eV are associated to $Zn2p_{3/2}$ and $Zn2p_{1/2}$, respectively [35,36]. The O1s XPS spectrum is asymmetry as observed from Fig. 4(c), indicating that at least two oxygen species are present in the nearby region. So we fit the spectra with Gaussian function and the deconvolutions show the presence of two different O1s peaks in the $Zn_{0.95}Y_{0.05}O$ nanoparticles. The peak centered at 531.0 eV is associated to the O^{2-} ion in the wurtzite structure surrounded by the Zn atoms with their full complement of nearest-neighbour O^{2-} ions [36–44], whereas the peak centered at 532.7 eV can be ascribed to the specific chemisorbed oxygen, such as $-CO_3$, adsorbed O_2, or adsorbed H_2O [36–44]. Fig. 4(d) shows the Y3d XPS spectrum. The peaks located at 159.7 eV and 157.8 eV are corresponding to the binding energy of $Y3d_{3/2}$ and $Y3d_{5/2}$, respectively, which clearly indicates that the Y ions have a +3 valence [45]. In comparison with the standard binding energy of $Y3d_{3/2}$ (157.4 eV) and $Y3d_{5/2}$ (156.6 eV) in Y_2O_3 [46,47], a blue shift of 2.3 eV and 1.2 eV in binding energy is observed for Y element in the $Zn_{0.95}Y_{0.05}O$ nanoparticles, which means the Y–O bond length in ZnO has changed due to Y^{3+} ions incorporating into the ZnO lattices, which is similar to the situation of ZnO:Tb thin films [48]. Moreover, the Y–O bond length should decrease when Y ions have been incorporated into the ZnO lattices and substituted the Zn^{2+} sites because the ionic radius of Y^{3+} is much bigger than that of Zn^{2+}. Such shrink of the Y–O bond length increases the interaction between ions and causes the slight blue shift in Fig. 4(d). This result, combined with the results of XRD and EDS, reveals that the Y dopants are successfully incorporated into ZnO lattices.

Fig. 5(a) shows the room temperature PL spectra of $Zn_{1-x}Y_xO$($x = 0, 0.03, 0.05$) nanoparticles. The samples are excited by a He–Cd laser with a wavelength of 325 nm. All the PL spectra in Fig. 5(a) consist of a UV peak at ~383 nm in wavelength and a very weak and broad deep level emission (DLE) band with a range from 500 nm to 600 nm. The UV emission band is related to a near band-edge transition of ZnO, namely, the recombination of the

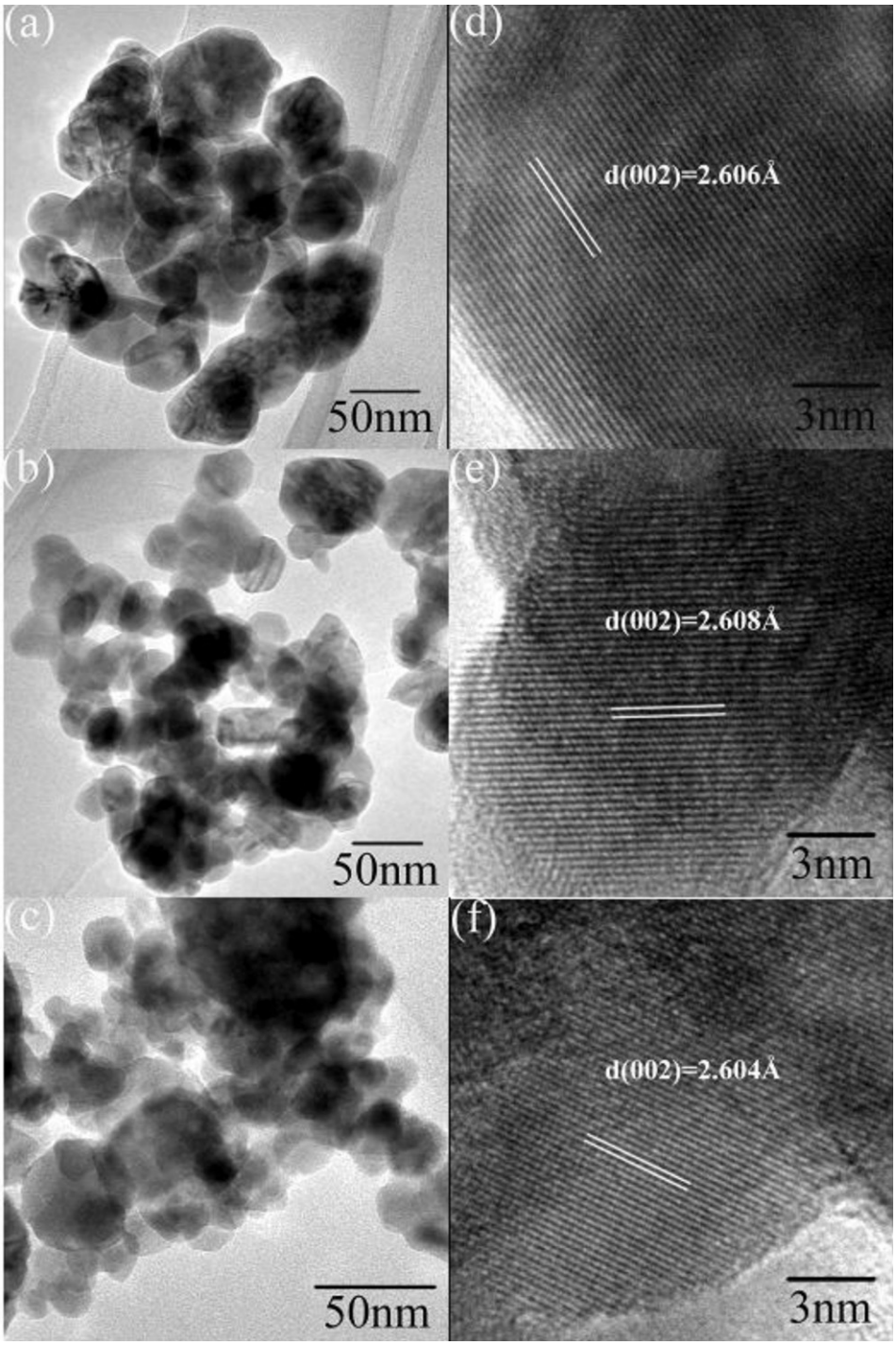

Fig. 2. TEM images of (a) pure ZnO, (b) $Zn_{0.97}Y_{0.03}O$, (c) $Zn_{0.95}Y_{0.05}O$; HETEM images of (d) pure ZnO, (e) $Zn_{0.97}Y_{0.03}O$, and (f) $Zn_{0.95}Y_{0.05}O$.

free excitons [49]. The deep-level emission band has previously been attributed to several defects in the crystal structure such as O-vacancy (V_O) [50,51], Zn-vacancy (V_{Zn}) [52], O-interstitial (O_i) [53], Zn-interstitial (Zn_i) [54], and extrinsic impurities such as substitutional Cu [55]. As shown in Fig. 5(a), the UV emission peak position located at 384.1 nm, 383.2 nm and 382.2 nm are corresponding to the samples with Y doping concentration of 0, 3% and 5%, respectively. Clearly, as Y doping concentration increases, the UV emission peak shifts to higher energy region. Since ZnO is usually a kind of n-type semiconductor material and Y ion is n-type dopant, this slight blueshift of UV emission can be ascribed to the Burstein–Moss effect [56]. Moreover, this result also has a good agreement with previous report by Kaur et al. [57], wherein they both theoretically calculated and experimentally testified that the value of bandgap energy (Eg) should increase after Y doping into ZnO crystal lattice.

Usually, the relative integrated PL intensity ratio between the UV emission (I_{UV}) and deep level emission (I_{DLE}) is used to characterize the optical properties of ZnO [58]. The larger intensity ratio indicates that ZnO has better optical properties, i.e., less deep level defects. From Fig. 5(a), we can observe that Y doping into the ZnO matrix could effectively enhance the UV emission. To see it clearly, I_{UV}/I_{DLE} as a function of various Y doping concentrations is clearly shown in Fig. 5(b). In our case, we use peak area to calculate the

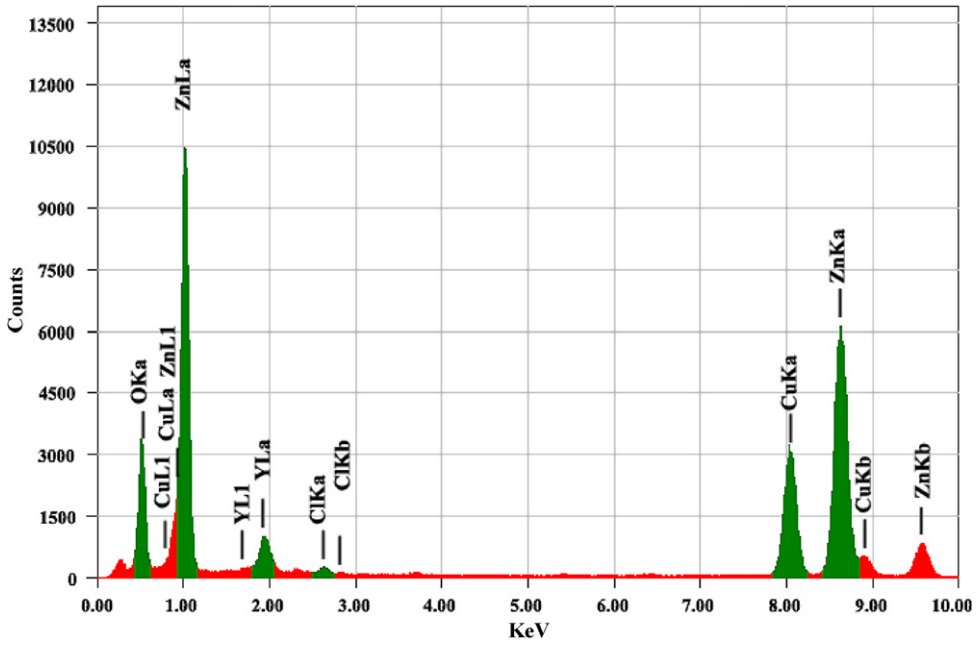

Fig. 3. EDS images of $Zn_{0.95}Y_{0.05}O$.

value of I_{UV}/I_{DLE}. The area of entire broad deep level emission in the range of 450–750 nm was used. It can be seen that the I_{UV}/I_{DLE} increases step by step as the increase of Y doping concentration, which means that Y doping makes the concentrations of some defects related to DLE band in $Zn_{1-x}Y_xO$ decrease.

Normally, the optical properties of ZnO are depending on the crystal quality. However, as discussed in XRD pattern (Fig. 1), we find that the crystal qualities of the samples turn worse with the incorporation of Y element. While, as shown in Fig. 5(a), the UV emission intensity is enhanced with the increase of Y-doping concentration. To explain this abnormal phenomena, we have to pay attention to the exciton recombination process in the semiconductor. As well as we known, under optical excitation, two competitive recombination processes exist in the materials, one is radiative

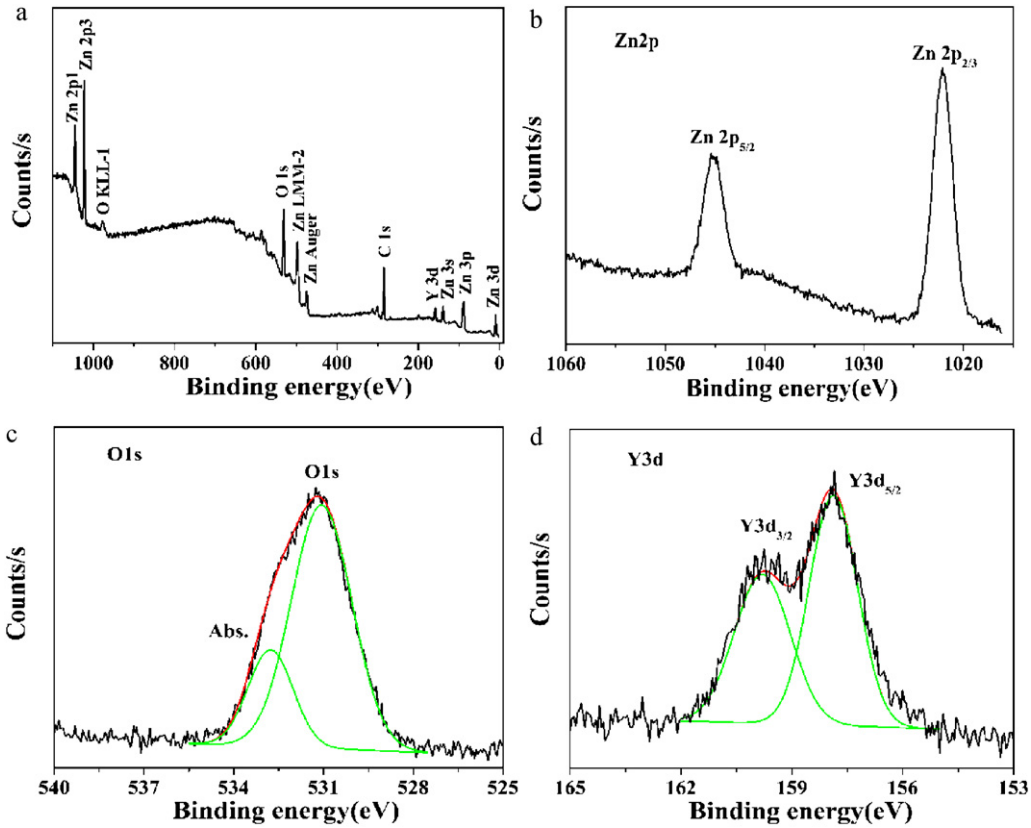

Fig. 4. XPS sepctra of $Zn_{0.95}Y_{0.05}O$. (a) XPS survey spectrum, (b) Zn 2p, (c) O1s, and (d) Y 3d.

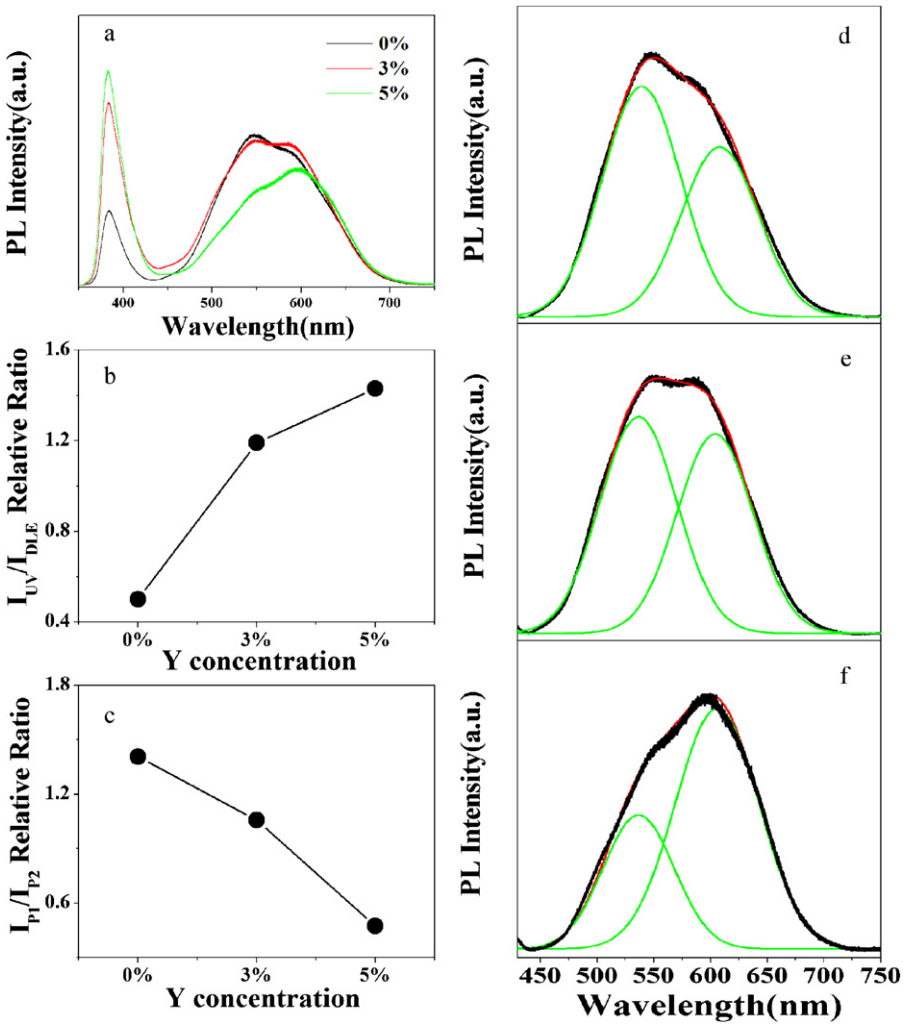

Fig. 5. (a) Room temperature PL spectra of the pure and Y-doped ZnO nanoparticles ($Zn_{1-x}Y_xO$, $x = 0, 0.03, 0.05$); (b) I_{UV}/I_{DLE} via Y doping concentration, (c) I_{P1}/I_{P2} via Y doping concentration; (d–f) Deep level emission of the pure and Y-doped ZnO nanoparticles fitted by Gaussian functions: (d) undoped, (e) $Zn_{0.97}Y_{0.03}O$, and (f) $Zn_{0.95}Y_{0.05}O$.

recombination and the other is nonradiative recombination. From this point of view, there are two kinds of defects in the samples, one is associated with a nonradiative transition and the other induces deep level emission. Both nonradiative recombinaton and deep level emission compete with UV emission. In our case, on one hand, Y doping into the ZnO crystal lattice will reduce the quantity of nonradiative recombination centers, which will depress the nonradiative recombination. On the other hand, the intensity of deep level emission also decreases, especially for the sample with 5% Y doping concentration, as show in Fig. 5(a). That is to say, Y doping can suppress two kinds of defects as indicated above and finally result in a stronger UV emission intensity in the PL spectra of Y-doped ZnO nanoparticles.

Moreover, the DLE band is very broad and asymmetric for all the samples. As shown in Fig. 5(d–f), a good fitting to the experimental data could be only obtained when deconvolutions of two Gaussians, centers at 539 nm and 598 nm, are used for the spectra, which indicates that two kinds of deep-level-defect luminescent centers exist in the samples. The green emission peak centered at 539 nm (named as P1) has been recently identified with different optical characteristics that at least two different defect origins, i.e., V_O and V_{Zn}, contribute to this band [50–52]. The emission peak centered at 598 nm (named as P2), is usually ascribed to the O_i or Li impurities [59,60]. However, in our case, there is no Li element in the samples as shown in Fig. 4(a). So we assume that O_i and the defects related to the Y element are supposed to be responsible for P2. Comparing three spectra in Fig. 5(d–f), the profiles change with Y doping concentration increasing from 0 to 5%, i.e., the peak position with maximum intensity is gradually tuned from P1 to P2. To see it clearly, the relative intensity ratio of I_{P1}/I_{P2} via a function of various Y doping concentrations is shown in Fig. 5(c), which clearly illustrates that the I_{P1}/I_{P2} value decreases step by step as the Y doping concentration increases from 0 to 5%. As mentioned above, V_O, V_{Zn}, and O_i should exist in the pure ZnO since both P1 and P2 present in the PL spectrum as shown in Fig. 5(d). After Y^{3+} is incorporated into ZnO lattices, a part of Y^{3+} will occupy the V_{Zn} position to lower the V_{Zn} concentration which finally results in the decrease of the P1 emission intensity. On the other hand, since Y ions exist in the ZnO lattices with +3 valence and they are apt to take the position of Zn ions which has a +2 valence, Y^{3+} is inevitable to attract more excess oxygen to be present in the O_i position so that the P2 emission will be enhanced. Therefore, P1 is gradually tuned to P2 and I_{P1}/I_{P2} value decreases step by step as the Y doping concentration increases from 0 to 5%.

Raman scattering is very sensitive to the microstructure of nanosized materials. It is a non-destructive characterization method for studying vibrational properties of ZnO nanostructures. The space group of the hexagonal wurzite ZnO belongs to C_{6v}^4, with two formula units per primitive cell. According to the group theory, single-crystalline ZnO has eight sets of optical phonon modes at Γ

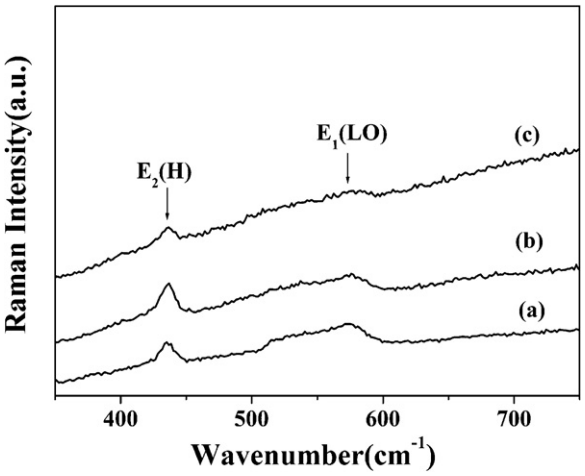

Fig. 6. Raman spectra of the pure and Y-doped ZnO nanoparticles. (a) undoped, (b) $Zn_{0.97}Y_{0.03}O$, and (c) $Zn_{0.95}Y_{0.05}O$.

point of the Brillouin zone, classified as $A_1 + E_1 + 2E_2$ modes (Raman active), $2B_1$ modes (Raman silent), and $A_1 + E_1$ modes (infrared active). Moreover, the A_1 and E_1 modes split into LO and TO components [61]. Fig. 6 shows the room temperature Raman spectra of the as-synthesized pure ZnO and $Zn_{1-x}Y_xO$ nanoparticles excited by the 514 nm line of an argon laser. The Raman peak at 436.8 cm^{-1} is attributed to the E_2(H) mode, which is one of the characteristic peaks of wurtzite structure of ZnO [62]. The peak located at 575 cm^{-1} is corresponding to E_1(LO) mode, which is usually ascribed to the formation of the defects such as oxygen vacancy and Zn interstitial [29,63,64]. Since the nanoparticles were casually dispersed on the sample holder for the Raman measurement, the quantity and thickness distribution of three samples were not exactly same during the measurement. From this piont of view, it is not accurate to compare the FWHM and intensity of single E_2(H) or E_1(LO) peak. Therefore, we use the relative intensity ratio between E_1(LO) or E_2(H) ($I_{E1(LO)}/I_{E2(H)}$) to characterize the structural properties of the samples. By using peak area, $I_{E1(LO)}/I_{E2(H)}$ was calculated to be 2.75, 1.91 and 1.84 corresponding to the samples with Y doping concentration of 0, 3% and 5%, respectively. Clearly, the relative intensity of E_1(LO) mode decreases as Y doping concentration increases from 0 to 5%, which further indicates that some defect concentration related to deep level emission might have been decreased so that the P1 emission will be depressed as revealed by the PL spectra.

4. Conclusions

In conclusion, Y-doped ZnO nanoparticles with wurtzite structure are successfully synthesized by the sol–gel technique. The results of structural characterization indicate that Y ions are incorporated into ZnO crystal lattices. PL spectra reveal that the optical properties of $Zn_{1-x}Y_xO$ nanoparticles turn better compared with pure ZnO nanoparticles due to the Y doping. With increasing Y-doping concentration, the intensity of UV emission can be strongly enhanced and the peak position with maximum intensity in deep-level emission band can be gradually tuned from 539 nm to 598 nm since the Y doping has redistributed the defects in the $Zn_{1-x}Y_xO$ nanoparticles. This obvious modulation of deep-level emission is incontrovertibly prompting the application of ZnO nanoparticles in full-color displays and photoelectric nanodevices. The growth technique also can be applied to introduce other rare-earth elements into ZnO nanoparticles with great advantages of easy operation and low cost.

Acknowledgements

This work is supported by the National Natural Science Foundation of China (Grant Nos. 60778040 and 60878039), Program for the development of Science and Technology of Jilin province (Item No. 20080151, 20090140 and 20100113), the Eleventh Five-Year Program for Science and Technology of Education Department of Jilin Province (Item No. 20090422 and 20100355), Program for the master students' scientific and innovative research of Jilin Normal University (Item No. S09010104) and the Open Project Program of National Laboratory of Superhard Materials (Item No. 201004).

References

[1] M. Willander, L.L. Yang, A. Wadeasa, S.U. Ali, M.H. Asif, Q.X. Zhao, O. Nur, J. Mater. Chem. 19 (2009) 1006.
[2] H.H. Huang, S.Y. Chu, P.C. Kao, Y.C. Chen, M.R. Yang, Z.L. Tseng, J. Alloys Compd. 479 (2009) 520.
[3] H. Yan, R. He, J. Johnson, M. Law, R.J. Saykally, P. Yang, J. Am. Chem. Soc. 125 (2003) 4728.
[4] P.L. Chen, X.Y. Ma, D.R. Yang, J. Alloys Compd. 431 (2007) 317.
[5] S.A.M. Lima, M.R. Davolos, C. Legnani, W.G. Quirino, M. Cremona, J. Alloys Compd. 418 (2006) 35.
[6] Y.X. Liu, C.F. Xu, Q.B. Yang, J. Appl. Phys. 105 (2009) 084701.
[7] A. Ishizumi, Y. Kanemitsu, Appl. Phys. Lett. 86 (2005) 253106.
[8] S.A.M. Lima, F.A. Sigoli, M.R. Davolos, M. Jafelicci Jr., J. Alloys Compd. 344 (2002) 280.
[9] J.H. Yang, J.H. Lang, L.L. Yang, Y.J. Zhang, D.D. Wang, H.G. Fan, H.L. Liu, X.Y. Wang, M. Gao, J. Alloys Compd. 450 (2008) 521.
[10] L.L. Yang, Q.X. Zhao, M. Willander, J.H. Yang, J. Cryst. Growth 311 (2009) 1046.
[11] R. Yousefi, M.R. Muhamad, A.K. Zak, Thin Solid Films 518 (2010) 5971.
[12] R. Yousefi, B. Kamaluddin, Appl. Surf. Sci. 255 (2009) 9376.
[13] R. Yousefi, B. Kamaluddin, Solid State Sci. 12 (2010) 252.
[14] R. Yousefi, M.R. Muhamad, J. Solid State Chem. 183 (2010) 1733.
[15] L.M. Kukreja, S. Barik, P. Misra, J. Alloys Compd. 268 (2004) 531.
[16] Y. Liu, J.H. Yang, Q.F. Guan, L.L. Yang, Y.J. Zhang, Y.X. Wang, B. Feng, J. Cao, X.Y. Liu, Y.T. Yang, M.B. Wei, J. Alloys Compd. 486 (2009) 835.
[17] A.K. Zak, W.H.A. Majid, M. Darroudi, R. Yousefi, Mater. Lett. 65 (2011) 70.
[18] A. Azam, F. Ahmed, N. Arshi, M. Chaman, A.H. Naqvi, J. Alloys Compd. 496 (2010) 399.
[19] S.S. Alias, A.B. Ismail, A.A. Mohamad, J. Alloys Compd. 499 (2010) 231.
[20] M. Ishii, S. Komuro, T. Morikawa, Y. Aoyagi, J. Appl. Phys. 89 (2001) 3679.
[21] T. Fukudome, A. Kaminaka, H. Isshiki, R. Saito, S. Yugo, T. Kimura, Nucl. Instrum. Methods Phys. Res., Sect. B 206 (2003) 287.
[22] Q.J. Yu, H.B. Yang, W.Y. Fu, L.X. Chang, J. Xu, C.L. Yu, R.H. Wei, K. Du, H.Y. Zhu, M.H. Li, G.T. Zou, Thin Solid Films 515 (2007) 3840.
[23] R. Kaur, A.V. Singh, R.M. Mehra, J. Non-Cryst. Solids 352 (2006) 2335.
[24] F.Y. Ran, L. Miao, S. Tanemura, M. Tanemura, Y. Cao, S. Tanaka, N. Shibata, Mater. Sci. Eng. B 148 (2008) 35.
[25] T.K. Jia, W.M. Wang, F. Long, Z.Y. Fu, H. Wang, Q.J. Zhang, Mater. Sci. Eng. B 162 (2009) 179.
[26] T.M. Hammad, J.K. Salem, R.G. Harrison, NANO 4 (2009) 225.
[27] P.K. Sharma, R.K. Dutta, A.C. Pandey, J. Magn. Magn. Mater. 321 (2009) 4001.
[28] X.Y. Fan, Y.X. Wang, Y.L. Zhang, L.K. Zeng, J. Synth. Cryst. 37 (2008) 1166.
[29] J. Lin, J.C. Yu, D. Lo, S.K. Lam, J. Catal. 183 (1999) 368.
[30] Y.S. Liu, W.Q. Luo, R.F. Li, G.K. Liu, M.R. Antonio, X.Y. Chen, J. Phys. Chem. C 112 (2008) 686.
[31] Ü. Özgür, Ya.I. Alivov, C. Liu, A. Teke, M.A. Reshchikov, S. Doğan, V. Avrutin, S.-J. Cho, H. Morkoç, J. Appl. Phys. 98 (2005) 041301.
[32] R.A. Laudise, A.A. Ballman, J. Phys. Chem. 64 (1960) 688.
[33] A. Al-Hajry, U. Ahmad, Y.B. Hahn, D.H. Kim, Superlattices Microstruct. 45 (2009) 529.
[34] S.Y. Bae, H.C. Choi, C.W. Na, J. Park, Appl. Phys. Lett. 86 (2005) 033102.
[35] T.L. Barr, M. Yin, S. Varma, J. Vaccine Sci. Technol. A 10 (1992) 2383.
[36] Y.F. Lu, H.Q. Ni, Z.H. Mai, Z.M. Ren, J. Appl. Phys. 88 (2000) 498.
[37] L.J. Meng, C.P. Moreira, M.P.D. Santos, Appl. Surf. Sci. 78 (1994) 57.
[38] E. De la Rosa, S. Seplveda-Guzman, B. Reeja-Jayan, A. Torres, P. Salas, N. Elizondo, M. Jose Yacaman, J. Phys. Chem. C 111 (2007) 8489.
[39] J.H. Lang, Q. Han, J.H. Yang, C.S. Li, X. Li, L.L. Yang, Y.J. Zhang, M. Gao, D.D. Wang, J. Cao, J. Appl. Phys. 107 (2010) 074302.
[40] D.K. Kim, H.B. Kim, J. Alloys Compd. 509 (2011) 421.
[41] R.K. Singhal, M.S. Dhawan, S.K. Gaur, S.N. Dolia, Sudhish Kumar, T. Shripathi, U.P. Deshpande, Y.T. Xing, S. Elisa, K.B. Garg, J. Alloys Compd. 477 (2009) 379.
[42] Y.X. Jin, Q.L. Cui, G.H. Wen, Q.S. Wang, J. Hao, S. Wang, J. Zhang, J. Phys. D: Appl. Phys. 42 (2009) 215007.
[43] D.D. Wang, G.Z. Xing, J.H. Yang, L.L. Yang, M. Gao, J. Cao, Y.J. Zhang, B. Yao, J. Alloys Compd. 504 (2010) 22.
[44] H.H. Wang, C.S. Xie, Phys. E 40 (2008) 2724.
[45] J.F. Moulder, W.F. Stickle, P.E. Sobol, K.D. Bomben, Handbook of X-ray Photoelectron Spectroscopy, Perkin Elmer Corp, Eden Prairie, MINN, 1992.
[46] G.M. Ingo, E. Paparazzo, O. Bagnarelli, N. Zacchetti, Surf. Interface Anal. 16 (1990) 515.

[47] C.D. Wagner, W.M. Riggs, L.E. Davis, J.F. Moulder, G.E. Muilenberg, Handbook of X-Ray Photoelectron Spectroscopy, Perkin-Elmer Corporation, Physical Electronics Division, Eden Prairie, MINN, 1979.
[48] X.M. Teng, H.T. Fan, S.S. Pan, C. Ye, G.H. Li, J. Appl. Phys. 100 (2006) 053507.
[49] D.M. Bengal, Y.F. Chen, Z. Zhu, T. Yao, Appl. Phys. Lett. 70 (1997) 2230.
[50] Q.X. Zhao, P. Klason, M. Willander, Appl. Phys. Lett. 87 (2005) 211912.
[51] T.M. Børseth, B.G. Svensson, A.Y. Kuznetsov, P. Klason, Q.X. Zhao, M. Willander, Appl. Phys. Lett. 89 (2006) 262112.
[52] P. Klason, T.M. Børseth, Q.X. Zhao, Solid State Commun. 145 (2008) 321.
[53] J. Zhong, A.H. Kitai, P. Mascher, W. Puff, J. Electrochem. Soc. 140 (1993) 3644.
[54] K. Johnston, M.O. Henry, D.M. Cabe, T. Agne, T. Wichert, Proceedings of the Second Workshop on SOXESS European Network on ZnO, Cearnarfon, Wales, UK 27–30, 2004.
[55] R. Dingle, Phys. Rev. Lett. 23 (1969) 579.
[56] Q.J. Yu, W.Y. Fu, C.L. Yu, H.B. Yang, R.H. Wei, Y.M. Sui, S.K. Liu, Z.L. Liu, M.H. Li, G.R. Wang, C.L. Shao, Y.C. Liu, G.T. Zou, J. Phys. D: Apple. Phys. 40 (2007) 5592.
[57] R. Kaur, A.V. Singh, R.M. Mehra, Phys. Stat. Sol. (a) 202 (2005) 1053.
[58] L.L. Yang, Q.X. Zhao, M. Willander, J.H. Yang, I. Ivanov, J. Appl. Phys. 105 (2009) 053503.
[59] Y.W. Heo, D.P. Norton, S.J. Pearton, J. Appl. Phys. 98 (2005) 073502.
[60] D. Li, Y.H. Leung, A.B. Djurisic, Z.T. Liu, M.H. Xie, S.L. Shi, S.J. Xu, W.K. Chan, Appl. Phys. Lett. 85 (2004) 1601.
[61] L.L. Yang, J.H. Yang, D.D. Wang, Y.J. Zhang, Y.X. Wang, H.L. Liu, H.G. Fan, J.H. Lang, Phys. E 40 (2008) 920.
[62] J.H. Yang, X.Y. Liu, L.L. Yang, Y.X. Wang, Y.J. Zhang, J.H. Lang, M. Gao, M.B. Wei, J. Alloys Compd. 485 (2009) 743.
[63] M.G. Zhao, X.C. Wang, L.L. Ning, H. He, J.F. Jia, L.W. Zhang, X.J. Li, J. Alloys Compd. 507 (2010) 97.
[64] A. Umar, S.H. Kim, J.H. Kim, A. Al-Hajry, Y.B. Hahn, J. Alloys Compd. 463 (2008) 516.